MATHEMATICAL METHODS IN THE APPLIED SCIENCES
Math. Meth. Appl. Sci. 2004; **27**:163–179 (DOI: 10.1002/mma.449)
MOS subject classification: 49 J 40; 49 Q 10; 49 Q 12; 73 M 25

Numerical simulation of the non-linear crack problem with non-penetration

Victor A. Kovtunenko*,†

Lavrent'ev Institute of Hydrodynamics, Novosibirsk 630090, Russia

Communicated by W. Wendland

SUMMARY

Here the numerical simulation of some plane Lamé problem with a rectilinear crack under non-penetration condition is presented. The corresponding solids are assumed to be isotropic and homogeneous as well as bonded. The non-linear crack problem is formulated as a variational inequality. We use penalty iteration and the finite-element method to calculate numerically its approximate solution. Applying analytic formulas obtained from shape sensitivity analysis, we calculate then energetic and stress characteristics of the solution, and describe the quasistatic propagation of the crack under linear loading. The results are presented in comparison with the classical, linear crack problem, when interpenetration between the crack faces may occur. Copyright © 2004 John Wiley & Sons, Ltd.

KEY WORDS: variational inequality; shape sensitivity analysis; fracture; interfacial crack; quasistatic crack propagation

1. INTRODUCTION

For concepts of cracks and their quasistatic propagation, we refer to the works [1–8]. Their methods of local asymptotic analysis and singular perturbation are employed, see also Reference [9]. A corresponding numerical algorithm for the simulation of the propagation of plane cracks can also be found in References [1,2].

Classically, problems with cracks are formulated as linear problems, based on the stress-free boundary condition on the crack faces. In this case, the interpenetration between the crack faces can occur, as we show in the example considered here. The non-linear model of cracks with the condition of non-penetration between the crack faces was first suggested by Khludnev in 1991. For some collection of such non-linear crack problems and their mathematical analysis, we refer to the recent book [10], which is devoted to the weak formulation of these problems as variational inequalities in the framework of variational theory and convex analysis.

*Correspondence to: Victor A. Kovtunenko, Lavrent'ev Institute of Hydrodynamics, Novosibirsk 630090, Russia.
†E-mail: kovtunenko@hydro.nsc.ru

Contract/grant sponsor: INTAS Foundation; contract/grant number: YSF 01/1-33

 Received 4 December 2001

On the other hand, methods of shape sensitivity analysis [11] were applied to the non-linear crack problems. In Reference [12], the derivative of the potential energy functional with respect to crack perturbation and the corresponding Cherepanov–Rice integral for the crack under the non-penetration condition have been presented. In the meantime, we extended these methods of shape sensitivity and optimization to various, linear and non-linear, crack problems. In References [13–15] we obtained the global asymptotic expansion of the solution, its stress and energetic characteristics, and suggested the quasistatic model of crack propagation.

Combining analytical formulas deduced in the works mentioned above, here we firstly realize the non-linear problem with crack under non-penetration condition numerically for the first time.

2. DATA FOR THE NUMERICAL TREATMENT

Let Ω be a unit square in $\mathbb{R}^2$ with the boundary Γ. We assume that Γ consists of two parts Γ_D and Γ_N. Let Ω consist of two subdomains Ω^+ and Ω^- with the interface Σ as shown in Figure 1. Here

$$\Omega^{\pm}=\{0<x_1<1,\quad 0<\pm x_2<0.5\},\quad \Sigma=\{0<x_1<1,\quad x_2=0\}$$
$$\Gamma_D=\{x_1=1,\quad -0.5<x_2<0.5\},\quad \Gamma_N=\Gamma_{N1}^{+}\cup\Gamma_{N2}^{+}\cup\Gamma_{N1}^{-}\cup\Gamma_{N2}^{-}$$
$$\Gamma_{N1}^{\pm}=\{x_1=0,\quad 0<\pm x_2<0.5\},\quad \Gamma_{N2}^{\pm}=\{0<x_1<1,\quad x_2=\pm 0.5\}$$

Let Γ_l be a part of the interface Σ of length l. We distinguish two opposite faces $\Gamma_l^{\pm}$ of Γ_l as shown in Figure 1, i.e.

$$\Gamma_l^{\pm}=\{0<x_1<l,\quad x_2=\pm 0\},\quad 0<l<1$$

Now define the domain $\Omega_l=\Omega\backslash\bar{\Gamma}_l$ in $\mathbb{R}^2$ with the boundary $\Gamma\cup\bar{\Gamma}_l^{+}\cup\bar{\Gamma}_l^{-}$. We will refer to Ω_l as a domain with the interfacial crack Γ_l. Namely, in each cross-section $x_3=\text{const}$, two solids occupy the domains Ω^+ and Ω^-, they are bonded at the part $\Sigma\backslash\Gamma_l$ of the interface, and the bonded solid has the crack Γ_l inside.

We now suppose plane stress distribution for our model. This implies for the displacement vector $u(x_1,x_2)=(u_1(x_1,x_2),u_2(x_1,x_2))$, that the stress and strain tensors have the components

$$\begin{aligned}\sigma_{ij}(u)&=2\mu^{\pm}\varepsilon_{ij}(u)+\lambda^{\pm}(\varepsilon_{11}(u)+\varepsilon_{22}(u))\delta_{ij}\\ \varepsilon_{ij}(u)&=\tfrac{1}{2}(u_{i,j}+u_{j,i}),\quad i,j=1,2\end{aligned}\tag{1}$$

Here, the Lamé parameters become

$$\mu^{\pm}=\frac{E^{\pm}}{2(1+\nu^{\pm})},\quad \lambda^{\pm}=\frac{E^{\pm}\nu^{\pm}}{(1+\nu^{\pm})(1-2\nu^{\pm})}\tag{2}$$

in each subdomain $\Omega^{\pm}$, respectively. For simplicity we assume that $\nu^-=\nu^-=\nu$ and $E^{\pm}=(1\pm b)E$ in (2). Then (2) takes the symmetric form

$$\mu^{\pm}=(1\pm b)\mu,\quad \lambda^{\pm}(1\pm b)\lambda,\quad \mu=\frac{E}{2(1+\nu)},\quad \lambda=\frac{E\nu}{(1+\nu)(1-2\nu)}$$

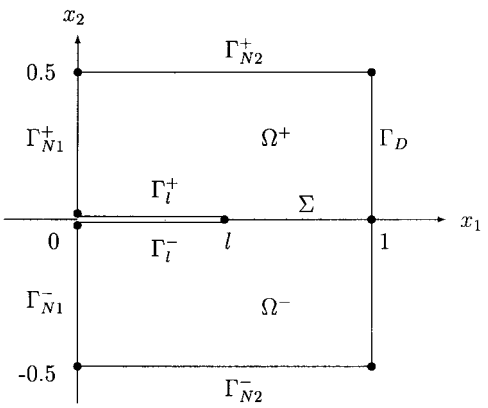

Figure 1. Domain Ω_l with the interfacial crack Γ_l.

In such way, the Lamé parameters are proportional to one parameter, called *bond* of the bonding as follows:

$$\frac{\mu^+}{\mu^-}=\frac{\lambda^+}{\lambda^-}=\frac{1+b}{1-b}=\text{bond} \tag{3}$$

In the numerical examples below we take the following particular values of material parameters

$$v=0.34, \quad E=7.3\times 10^4 \text{ mPa}$$

Let us consider first that the body is homogeneous, i.e. $b=0$ and $bond=1$ in (3). The case of a bonded solid will be treated separately in Section 7.

We investigate the following problem. The equilibrium equations hold inside either domain:

$$\sigma_{ij,j}(u)=0, \quad i=1,2 \quad \text{in } \Omega^{\pm} \tag{4}$$

The transmission conditions are assumed to be fulfilled at the connected part of the interface:

$$[\![u_i]\!]=0, \quad [\![\sigma_{i2}(u)]\!]=0, \quad i=1,2 \quad \text{on } \Sigma\backslash\Gamma_l \tag{5}$$

Here the brackets $[\![\cdot]\!]$ denote the jump across the interface. At the part Γ_D of the external boundary we assume the following mixed conditions:

$$u_1=0, \quad \sigma_{12}(u)=0 \quad \text{on } \Gamma_D \tag{6}$$

Relations (6) can be interpreted as the condition of symmetry with respect to the edge $\{x_1=1\}$ for the symmetric prolongation of the solid onto the half-plane $\{x_1>1\}$. To neglect rigid displacements $u_2=\text{const}$, which are admissible under the boundary conditions (6), we fix one point, for instance,

$$u_2(1,0)=0$$

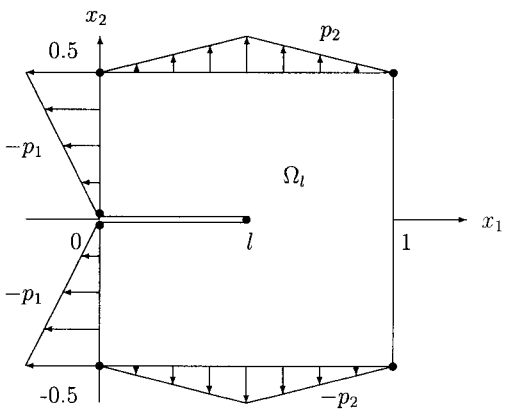

Figure 2. Traction forces applied at Γ_N.

At the boundary Γ_N we impose symmetric loading by the following traction forces:

$$g_1 = -p_1, \quad g_2 = 0 \quad \text{on } \Gamma_{N1}^{\pm} \tag{7}$$

$$g_1 = 0, \quad g_2 = \pm p_2 \quad \text{on } \Gamma_{N2}^{\pm} \tag{8}$$

with the piecewise-linear functions

$$p_1(x_2) = t_0\mu\, 13|x_2|, \quad p_2(x_1) = t_0\mu\,(1 - |2x_1 - 1|), \quad t_0 = 0.9 \times 10^{-3} \tag{9}$$

as shown in Figure 2. The constants chosen give us the dimensional evaluation of the load in (9) as follows:

$$\max\{p_1\} \approx 160\ \text{mPa}, \quad \max\{p_2\} \approx 24.5\ \text{mPa}$$

If we apply only the loading p_2 from (8), i.e. $p_1 = 0$ in (7), this leads to an opening of the crack Γ_l. Inversely, if we apply only the loading p_1 from (7) with $p_2 = 0$ in (8), this causes the interpenetration between the crack faces $\Gamma_l^{\pm}$. In our case, we employ a competition between the two loading p_1 and p_2. The choice of the constants in (9) implies that $\max\{p_2\}$ is about 15% of $\max\{p_1\}$.

For numerical calculations we apply the finite-element method. By this we construct the uniform triangular mesh as shown in Figure 3. Taking H points along each, the x_1 and x_2 directions, there are defined $(H-1)^2$ equal squares of the size

$$h = \frac{1}{H-1} \tag{10}$$

Each of them is split into two triangles. At the crack Γ_l of length $l = Ch$ we have C double nodes with $2 \leqslant C \leqslant H - 3$. The splitting of squares is chosen in such a way that there are 10-points of finite elements near the crack tip. At each triangle we use linear approximation of displacements u. By testing the whole piecewise-linear finite-element approximation of the cracked domain for the exact solution of a corresponding Laplace problem with crack,

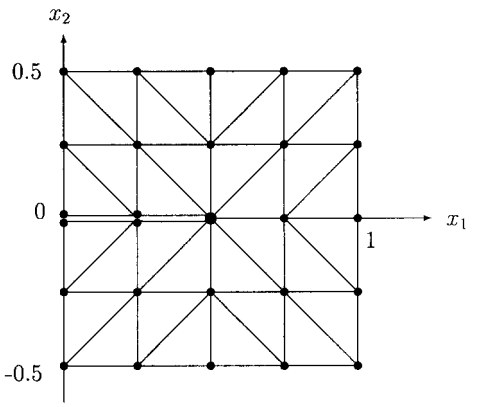

Figure 3. Triangular mesh on Ω_l for $H=5$ and $C=2$.

in Reference [16] we get the speed of convergence of the energy error, which is linear with respect to the mesh size h from (10).

3. LINEAR PROBLEMS WITH STRESS-FREE CRACK FACES

Let us assume the classical stress-free boundary condition at the crack Γ_l:

$$\sigma_{i2}(u)=0, \quad i=1,2 \quad \text{on } \Gamma_l^{\pm} \tag{11}$$

Introduce the space

$$\tilde{H}^1(\Omega_l) \subset \{u=(u_1,u_2)\in[H^1(\Omega_l)]^2, \quad u_1=0 \quad \text{on } \Gamma_D\}$$

which is orthogonal to rigid displacements $\{u=(u_1,u_2),\ u_1\equiv 0,\ u_2\equiv c\}$. We define the weak solution of problem (4)–(8), (11) from the variational equation

$$\int_{\Omega_l}\sigma_{ij}(u^l)\varepsilon_{ij}(v)=\int_{\Gamma_N} g_i v_i \quad \forall v\in\tilde{H}^1(\Omega_l) \tag{12}$$

By the index l we mark the one-parametric dependence of the solution on the crack length, that we will investigate in what follows.

From (12), the function P of potential energy of the solid can be defined (in cross-section $x_3=\text{const}$) in dependence on the crack length l, i.e.

$$P(l)=\frac{1}{2}\int_{\Omega_l}\sigma_{ij}(u^l)\varepsilon_{ij}(u^l)-\int_{\Gamma_N} g_i u_i^l \text{ mPa m}^2 \tag{13}$$

where $0<l<1$. To calculate (13), one needs to solve problem (12) for every value of l. Under the data from Section 1, numerical values of the potential energy $P(l)$ for the linear problem are presented in Figure 7 for the number $H=41$ from (10). As mentioned before, we assume here that the energy error of approximation has the order h.

To calculate the first derivative of the potential energy with respect to the perturbation of the crack length (energy release rate), we apply the analytical formulas from References

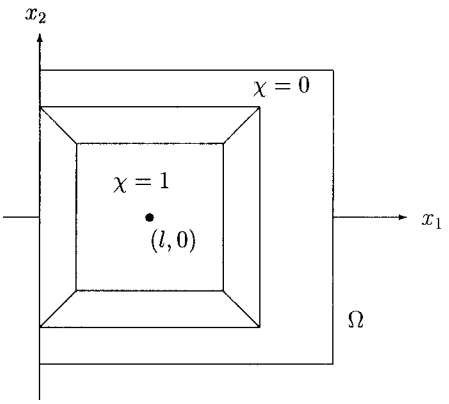

Figure 4. View from above of the cut-off function χ.

[14,15]. Take some arbitrary cut-off function $\chi \in W^{1,\infty}(\Omega)$ with $\chi \equiv 1$ near the crack tip, and $\chi \equiv 0$ near the external boundary Γ. Then the first derivative has the representation

$$P'(l) = \frac{1}{2} \int_{\Omega_l} A^1(\chi; u^l, u^l) \text{ mPa m} \tag{14}$$

where the symmetric bilinear form $A^1(\chi; \cdot, \cdot)$ is given by

$$\begin{aligned} A^1(\chi; u, v) &= \chi_{,1}\sigma_{ij}(u)\varepsilon_{ij}(v) - \sigma_{ij}(u)E_{ij}(\chi; v) - \sigma_{ij}(v)E_{ij}(\chi; u) \\ E_{ij}(\chi; u) &= \tfrac{1}{2}(\chi_{,i}u_{j,1} + \chi_{,j}u_{i,1}), \quad i,j = 1,2 \end{aligned} \tag{15}$$

Its numerical value calculated for $H = 41$ is presented in Figure 8. Note that, integrating by parts, with the help of relations (4) and (11), the integral over the domain in (14) can be rewritten in equivalent form of the well-known path-independent Cherepanov–Rice integral

$$P'(l) = \int_B \left(-\frac{1}{2}\, \sigma_{ij}(u^l)\varepsilon_{ij}(u^l)\eta_1 + \sigma_{ij}(u^l)\eta_j u^l_{i,1} \right) \tag{16}$$

over any closed contour B surrounding the crack tip, with the normal vector (η_1, η_2) to B. It has been proved rigorously, that the integral representation (14) does not depend on the cut-off function χ, like the equivalent representation (16). For the numerical approximation we take the piecewise-linear functions χ as illustrated in Figure 4.

We treat the stress intensity factors (SIF) as some integral form over the solution, too. In the polar co-ordinates near the crack tip

$$x_1 - l = r\cos\phi, \quad x_2 = r\sin\phi, \quad r \geqslant 0, \quad |\phi| \leqslant \pi$$

consider the well-known singular functions for the homogeneous body

$$\begin{aligned} \Phi^1 &= \sqrt{r}((2\kappa - 1)\cos\tfrac{\phi}{2} - \cos\tfrac{3\phi}{2}, (2\kappa + 1)\sin\tfrac{\phi}{2} - \sin\tfrac{3\phi}{2}) \\ \Phi^2 &= \sqrt{r}((2\kappa + 3)\sin\tfrac{\phi}{2} + \sin\tfrac{3\phi}{2}, -(2\kappa - 3)\cos\tfrac{\phi}{2} - \cos\tfrac{3\phi}{2}), \quad \kappa = \tfrac{3\mu+\lambda}{\mu+\lambda} \end{aligned}$$

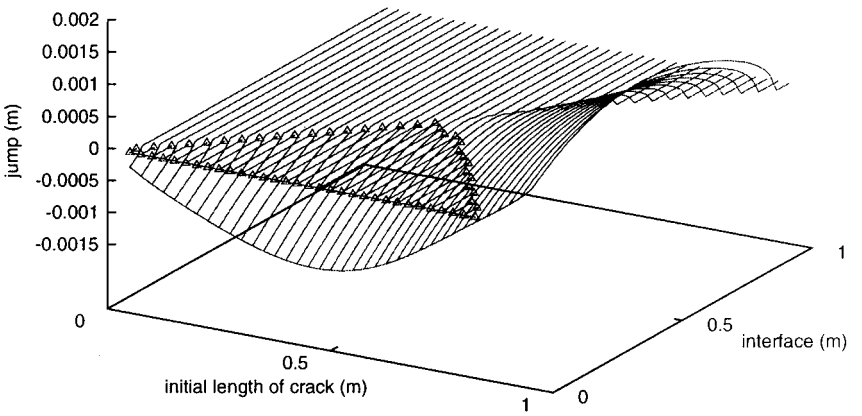

Figure 5. Jump $[\![u_2^l]\!]$ at Σ for the linear problem.

We have to solve two auxiliary problems with the singular functions Φ^1 and Φ^2 in the right-hand side and A^1 from (15) as follows:

$$\int_{\Omega_l} \sigma_{ij}(V^k(\chi;l))\varepsilon_{ij}(v) = -\int_{\Omega_l} A^1(\chi;\Phi^k,v) \quad \forall v \in \tilde{H}^1(\Omega_l), \quad k=1,2$$

to find its solutions $V^k(\chi;l) \in \tilde{H}^1(\Omega_l)$. This problem is analogous to (12) and differs from it only by the right-hand side, which describes some fictitious forces. Then the SIFs can be represented explicitly in the form of integrals, in our case due to $\chi = 0$ at Γ, in the form

$$K_k(l) = \frac{\mu+\lambda}{2\sqrt{2\pi}(2\mu+\lambda)} \int_{\Gamma_N} g_i V_i^k(\chi;l), \quad k=1,2 \text{ mPa } \sqrt{\text{m}}$$

which is independent of the cut-off function χ. Executing numerically the formulas shown above, under the loading from (7)–(8) we have found $K_2(l) \equiv 0$, and $K_1(l)$ as presented in Figure 9. Let us also recall here the well-known physical relation connecting the SIF with the first derivative of the potential energy:

$$P'(l) = -\frac{\mu(1-\nu)}{2} K(l)^2, \quad K(l) = \sqrt{K_1(l)^2 + K_2(l)^2} \tag{17}$$

Mathematically, problem (12) is correct. Let us consider now the jump $[\![u_2^l]\!]$ at the interface Σ, which is numerically calculated for all values of the crack length l and shown in Figure 5. We can see marked here the interpenetration zone at the crack Γ_l where $[\![u_2^l]\!] < 0$, that, of course, is unacceptable from the physical point of view. The choice of loading p_1 and p_2 from (7) and (8) in our example provides all possible cases depending on the length of the crack. We find full interpenetration between the crack faces for small l: full opening of the crack close to the edge $\{x_1 = 1\}$; and both interpenetration and opening, inside.

4. NON-LINEAR PROBLEMS WITH NON-PENETRATION CONDITION

We now formulate the model providing non-penetration between crack faces, i.e.

$$[\![u_2]\!] \geqslant 0 \quad \text{on } \Gamma_l \tag{18}$$

Let us introduce the set of admissible displacements

$$K_l = \{u = (u_1, u_2) \in \tilde{H}^1(\Omega_l), \quad u \text{ satisfies (18)}\}$$

and consider the variational inequality

$$\int_{\Omega_l} \sigma_{ij}(u^l)\varepsilon_{ij}(v - u^l) \geqslant \int_{\Gamma_N} g_i(v_i - u_i^l) \quad \forall v \in K_l \tag{19}$$

Its solution $u^l \in K_l$ describes the equilibrium problem (4)–(8) with the boundary condition at the crack as follows:

$$\begin{aligned} &[\![\sigma_{i2}(u^l)]\!] = 0, \quad i = 1, 2, \quad \sigma_{12}(u^l) = 0 \quad \text{on } \Gamma_l \\ &[\![u_2^l]\!] \geqslant 0, \quad \sigma_{22}(u^l) \leqslant 0, \quad [\![u_2^l]\!]\sigma_{22}(u^l) = 0 \quad \text{on } \Gamma_l \end{aligned} \tag{20}$$

In what follows we will consider non-penetration conditions (20) instead of the stress-free condition (11), and the corresponding non-linear problem (19) instead of the linear problem (12).

To find an approximate solution of the variational inequality (19), we apply the iteration penalty method and use theoretical results, presented in Reference [10]. First, for small parameter $\delta > 0$, we consider the non-linear penalty equation

$$\int_{\Omega_l} \sigma_{ij}(u^l(\delta))\varepsilon_{ij}(v) - \frac{1}{\delta}\int_{\Gamma_l} [\![u_2^l(\delta)]\!]^- [\![v_2]\!] = \int_{\Gamma_N} g_i v_i \quad \forall v \in \tilde{H}^1(\Omega_l) \tag{21}$$

where the upper minus denotes the negative part of the corresponding function, namely,

$$[\![u]\!]^- = \max\{0, -[\![u]\!]\} = \begin{cases} 0 & \text{if } [\![u]\!] \geqslant 0 \\ -[\![u]\!] & \text{if } [\![u]\!] < 0 \end{cases}$$

Then solutions of problem (21) converge to the solution of problem (19), see Reference [10]:

$$\|u^l(\delta) - u^l\|_{H^1} \to 0 \quad \text{as } \delta \to 0$$

with the order $\sqrt{\delta}$ of the convergence. Second, we linearize (21) with the help of iterations as follows:

$$\begin{aligned} &\int_{\Omega_l} \sigma_{ij}(u^l(\delta, n))\varepsilon_{ij}(v) + \frac{1}{\delta}\int_{\Gamma_l} [\![u_2^l(\delta, n) - u_2^l(\delta, n-1)]\!]\, [\![v_2]\!] \\ &\quad = \int_{\Gamma_N} g_i v_i + \frac{1}{\delta}\int_{\Gamma_l} [\![u_2^l(\delta, n-1)]\!]^- [\![v_2]\!] \quad \forall v \in \tilde{H}^1(\Omega_l) \end{aligned} \tag{22}$$

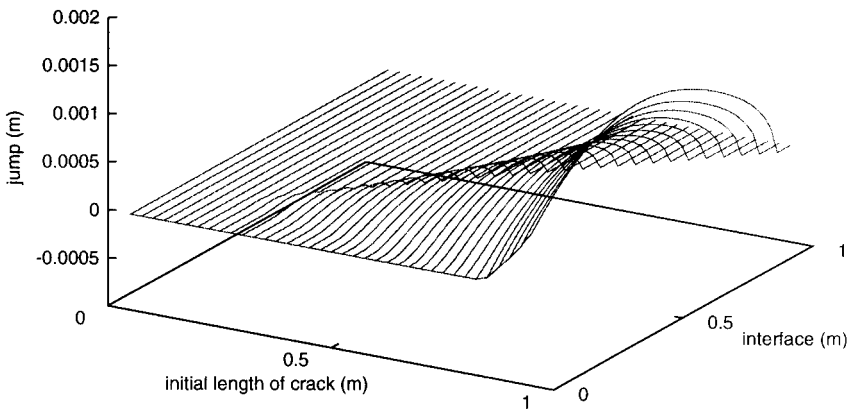

Figure 6. Jump $[\![u_2^l]\!]$ at Σ for the non-linear problem.

The following estimate was proved in Reference [10]:

$$\|u^l(\delta,n)-u^l(\delta)\|_{H^1} \leqslant \left(\frac{1}{1+c\delta}\right)^{n/2} \|u^l(\delta,0)-u^l(\delta)\|_{H^1}$$

which provides the convergence of the solutions of problem (22) to the solution of problem (21) as $n\to\infty$. Thus, we can use the two-level approximate model (22) for seeking the approximate solution of the variational inequality (19). In our numerical computations, we use such values of parameters of the approximation, which suggest theoretically an error within 5% in the H^1-norm.

Realizing numerical calculations of problem (19) by the above scheme, we found the jump $[\![u_2^l]\!]$ at the crack Γ_l as presented in Figure 6 (compare with Figure 5). We see here the full contact for small crack length l, full opening for l close to 1, and both contact and opening, inside. Of course, such picture is physically more preferable to the situation in Figure 5.

5. POTENTIAL ENERGY AND ITS DERIVATIVE

Let us define the function P of potential energy from the solution u^l of the non-linear problem (19) by

$$P(l)=\frac{1}{2}\int_{\Omega_l}\sigma_{ij}(u^l)\varepsilon_{ij}(u^l)-\int_{\Gamma_N}g_i u_i^l \text{ mPa m}^2 \tag{23}$$

Its numerical values calculated for various numbers $H=11,21,41$ from (10) are presented in Figure 7. Here we see the relative convergence of the energy when refining the mesh, i.e. increasing H. Supposing linear speed of convergence in h, in what follows we choose $H=41$ (i.e. the mesh size $h=0.025$) which provides us enough accuracy of our calculations. For comparison, we also present the potential energy from (13) for the linear problem with crack.

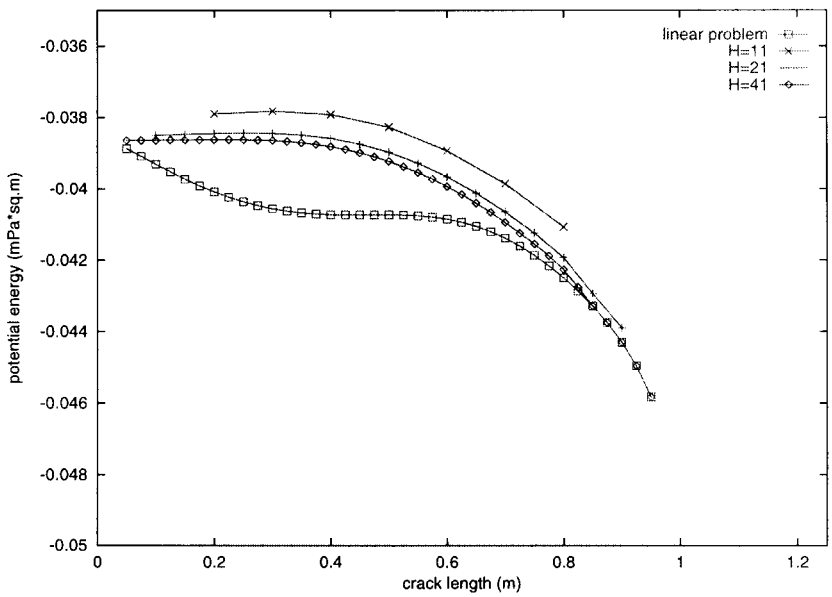

Figure 7. Function $P(l)$ of the potential energy.

In References [10,12,13] the integral representation of the first derivative of the potential energy with respect to the perturbation of the crack length l is given in the form

$$P'(l) = \frac{1}{2} \int_{\Omega_l} A^1(\chi; u^l, u^l) \,\mathrm{mPa\,m} \tag{24}$$

with the symmetric bilinear form $A^1(\chi; \cdot, \cdot)$ from (15). Formula (24) appears to be analogous to (14) for the linear problem. Again, there was proved the independence of representation (24) of the cut-off function χ and its equivalence to the path-independent integral over contour of form (16). The numerically calculated values of $P'(l)$ are presented in Figure 8 when refining the mesh and in comparison with the corresponding values from (14) for the linear problem. Up to a small error of approximation, in Figure 8 we can see the interval $0 < l < l^*$, $l^* \approx 0.25$, where $P'(l) = 0$.

Formula (24) remains valid for bonded solids, too, due to the differentiation along the interface.

In spite of the seemingly full analogy with the linear problem, we fail to attain the derivative $P'(l)$ for curvilinear cracks under the non-penetration conditions.

6. SIF-SIZED PARAMETER

For the non-linear crack problem (19), the non-positiveness property of $P'(l)$ can be easily proved. Therefore, we can formally define the SIF-sized parameter $K(l) \geqslant 0$ from the derivative

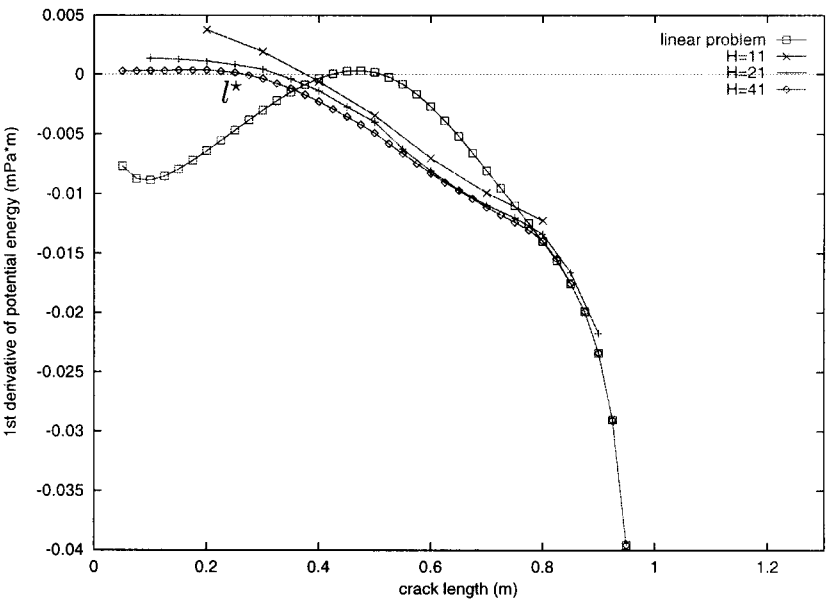

Figure 8. First derivative $P'(l)$ of the potential energy.

of potential energy, which yields the equality (17), namely

$$K(l) = \sqrt{\frac{-2P'(l)}{\mu(1-\nu)}}\ \text{mPa}\sqrt{\text{m}} \tag{25}$$

For the linear problem from Section 2, due to $K_2(l) \equiv 0$, the SIF-sized parameter $K(l)$ defined by (25) is exactly equal to $K_1(l)$. Both these parameters for our example for the data from Section 1 are presented in Figure 9.

Again, in Figure 9, we see the negative values of $K_1(l)$ for the linear problem, which have no physical meaning.

7. QUASISTATIC PROPAGATION OF CRACKS

Fix some initial crack length l_0 with $0 < l_0 < 1$. For the dimensionless loading parameter t, suppose the linear loading process

$$g_1(t) = t\, g_1, \quad g_2(t) = t\, g_2, \quad t \geqslant 0 \tag{26}$$

with functions g_1 and g_2 from (7), (8). In analogy with (19), let us consider the quasistatic equilibrium problem under loading from (26):

$$\int_{\Omega_{l_0}} \sigma_{ij}(u^{l_0}(t))\varepsilon_{ij}(v - u^{l_0}(t)) \geqslant \int_{\Gamma_N} g_i(t)(v_i - u_i^{l_0}(t)) \quad \forall v \in K_{l_0} \tag{27}$$

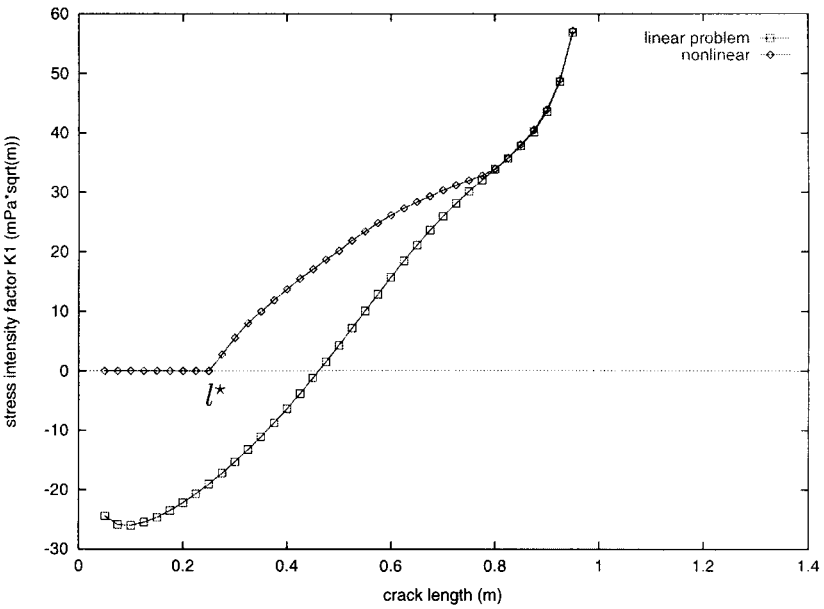

Figure 9. SIF-sized parameter $K(l)$.

Due to the cone property of the set K_{l_0}, we have

$$u^{l_0}(t) = tu^{l_0} \in K_{l_0} \tag{28}$$

for the solution of (27). Thanks to (28), it follows evidently from (23) and (24) that the potential energy corresponding to (27) and its derivative have the values

$$P(l_0,t) = t^2 P(l_0), \quad P'(l_0,t) = t^2 P'(l_0) \tag{29}$$

The Griffith fracture criterion implies that

$$\gamma + P'(l_0,t) > 0 \Rightarrow \text{no crack growth} \tag{30}$$

$$\gamma + P'(l_0,t) = 0 \Rightarrow \text{initiating of growth} \tag{31}$$

where the positive constant $\gamma > 0$ means the doubled density of the surface energy at the crack. For numerical calculations we take the following value of γ:

$$\gamma = \frac{K_{3\,\mathrm{cr}}^2}{2\mu}\ \mathrm{mPa\,m}, \quad K_{3\,\mathrm{cr}} = 25\ \mathrm{mPa}\sqrt{\mathrm{m}}, \quad \gamma \approx 0.011$$

that corresponds to the mode-3 case treated in Reference [16]. Due to (29) and $P'(l_0) < 0$, we have $\gamma + P'(l_0,t) = \gamma + t^2 P'(l_0)$ which is a decreasing function of t.

Therefore, it follows from (30) that the crack of initial length l_0 does not grow under the linear loading (26) inside $0 \leqslant t < t_{\mathrm{cr}}(l_0)$. This critical value of t can be found from (31) by solving the equation

$$\gamma + t_{\mathrm{cr}}^2(l_0) P'(l_0) = 0$$

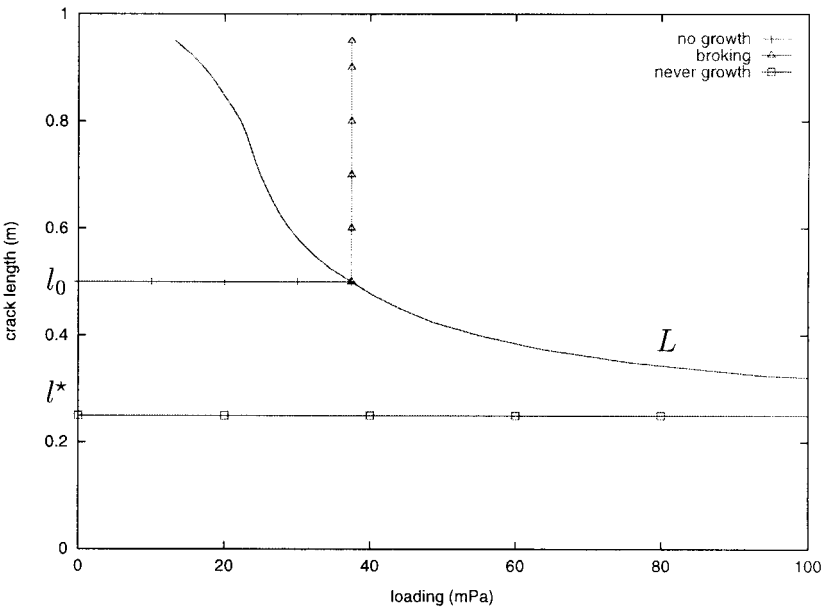

Figure 10. Quasistatic propagation of the crack.

It gets the value

$$t_{\mathrm{cr}}(l_0) = \sqrt{\frac{\gamma}{-P'(l_0)}} \tag{32}$$

due to $P'(l_0) < 0$. Following (9), let us now define from (32) the dimensional function of critical loading p_{cr} in dependence on the initial crack length l_0 by

$$p_{\mathrm{cr}}(l_0) = t_0 \mu \sqrt{\frac{\gamma}{-P'(l_0)}}\ \mathrm{mPa} \tag{33}$$

This physical value is equal to the maximum of the applied loading p_2, while the maximum of the corresponding loading p_1 is 6.5 times more in view of definition (9). Using numerical values of the derivative $P'(l)$ from (24) as $H = 41$, we construct the function $p = p_{\mathrm{cr}}(l)$ from (33) as presented in Figure 10 and marked by L.

Having the whole curve L of the critical loading, we can now describe the global process of quasistatic crack propagation which we base on two main assumptions: the loading grows linearly; and the crack can extend only in view of the Griffith fracture hypothesis. This process is illustrated in Figure 10 for the initial crack length $l_0 = 0.5$. At the first step there is no growth until $\max\{p_2(t)\} = \max\{p_1(t)\}/6.5 = p_{\mathrm{cr}}(l_0)$, in Figure 10 see $p_{\mathrm{cr}}(0.5) \approx 37.5$ mPa. Then the crack growth with infinite velocity occurs at $p_{\mathrm{cr}}(l_0)$, which should mean immediate breaking of the solid along the interface. This situation takes place for initial crack lengths $l_0 > l^*$, in Figure 10 see $l^* \approx 0.25$. The other case $0 < l_0 < l^*$ corresponds to the interval in Figure 8 where $P'(l_0) = 0$. In view of (33), for $l_0 < l^*$ we have no growth at all, the crack Γ_{l_0} remains closed.

Thus, the propagation of cracks with possible contact between the crack faces and under linear loading can be in our example either unstable with breaking, or does not occur at all, depending on the initial crack length.

Note, property (28) also implies that the zone of contact between the crack faces, where $[\![u_2^l]\!] = 0$, remains unchanged until the crack begins to grow.

8. BONDED SOLID

Now we consider a bonded solid Ω_l with an interfacial crack Γ_l between different homogeneous isotropic materials in $\Omega^{\pm}$. We distinguish these materials with the help of the parameter *bond* introduced in (3). In particular, we vary the value $bond = 1, 1.5, 2, 2.5, 3$. For comparison, the case $bond = 1$ corresponds to the homogeneous body investigated in previous sections.

First, consider the function of potential energy $P(l)$ introduced in (23) and its derivative. All formulas from Section 4 remain valid for the bonded solid due to the differentiation along the interface. Solving numerically problem (19) with $H = 41$ for various numbers of *bond* and for all discrete values of the crack length l, we substitute the corresponding solutions into integral (23) to see the curves of potential energy $P(l)$ in Figure 11.

The analytic formula (24) gives us the first derivative $P'(l)$ of the corresponding curves from Figure 11, which are presented in Figure 12.

By applying formula (25), from the first derivative $P'(l)$ we calculate the SIF-sized parameter $K(l)$ presented in Figure 13.

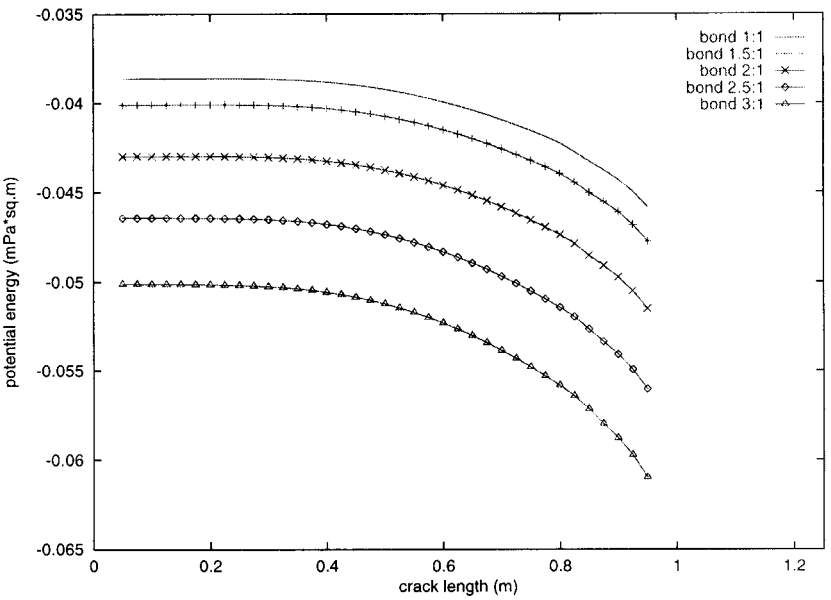

Figure 11. Potential energy $P(l)$ for a bonded solid.

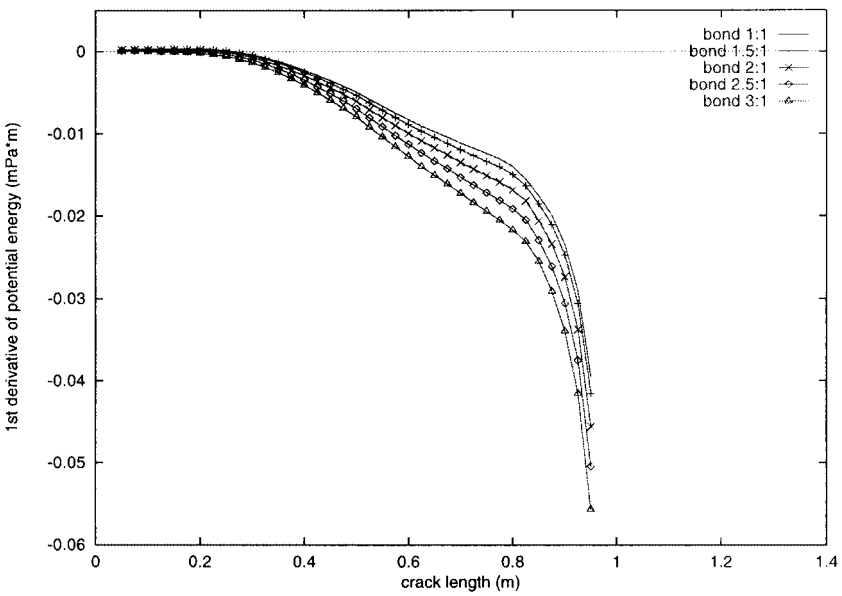

Figure 12. First derivative $P'(l)$ for a bonded solid.

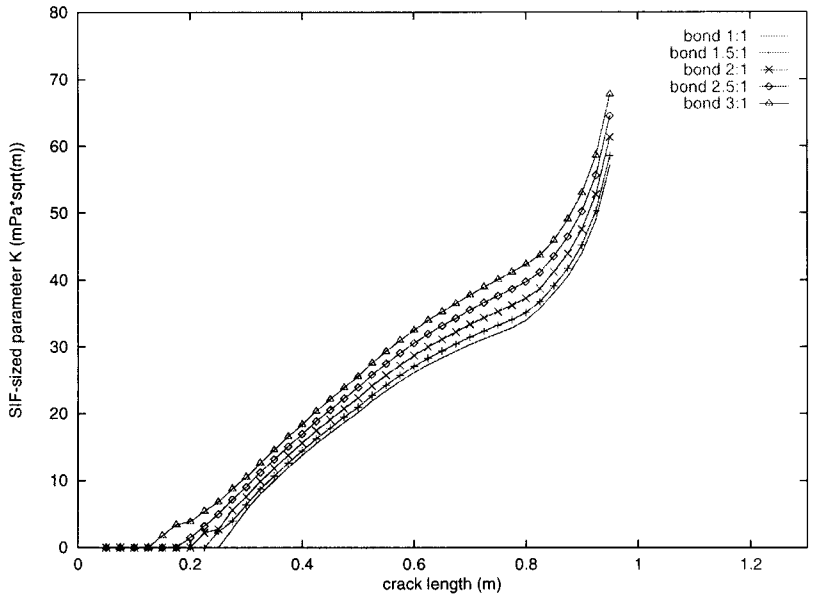

Figure 13. SIF-sized parameter $K(l)$ for a bonded solid.

Assuming that the delamination process takes place in the bonded solid, we find the curves of critical loading for the straight-line crack propagation from (33), which are calculated in Figure 14.

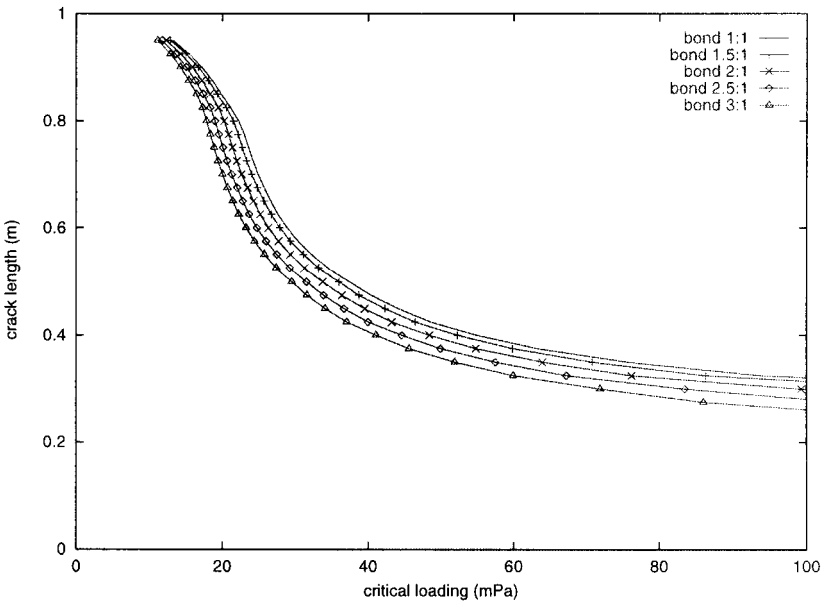

Figure 14. Critical loading $p_{\rm cr}(l)$ for delamination.

9. CONCLUSION

When we suppose the classical stress-free boundary condition at the crack, the interpenetration between crack faces can occur as in the example considered, which is unacceptable from physic's point of view. The linear model can be corrected by assuming that the non-penetration condition is fulfilled at the crack. Applying the shape sensitivity and optimization methods, for rectilinear cracks we find the functions of potential energy and its first derivative, SIF-sized parameters depending on the crack length, and describing the quasistatic propagation of the crack along the straight-line interface. In our example, the crack does not grow, or, its growth is unstable with breaking, depending on the initial length of crack. Bonded solids with crack along the interface can be treated within this approach, too.

ACKNOWLEDGEMENTS

These research results were obtained with support of the INTAS Foundation in the framework of the research grant YSF 01/1-33, and while visiting Professor W.L. Wendland at the Mathematical Institute A of the University of Stuttgart.

REFERENCES

1. Bach M. Randvariationsungleichungen zur Beschreibung des quasistatischen Rißwachstums eines ebenen 3D-Risses in isotropem Material. *Doctoral Thesis* (PhD), Stuttgart University, 1998.
2. Bach M, Nazarov SA, Wendland WL. Stable propagation of a mode-1 planar crack in an anisotropic elastic media. Comparison of the Irwin and the Griffith approaches. In *Problemi Attuali dell'Analisie della Fisica Mathematica*, Ricci PE (ed.). MM ARACNE EDITRICE: Roma, 2000; 167–189.

3. Bochniak M, Sändig A-M. Sensitivity analysis of 2D interface cracks. In *Proceedings of the Conference on PDE Multistructures*, *Luminy*, 1999. Ali Mahmeti F, von Below J, Nicaise S (eds). Marcel Dekker Inc.: New York, 2001.
4. Duduchava R, Sändig A-M, Wendland WL. Interface cracks in anisotropic materials. *Mathematical Methods in the Applied Sciences* 1999; **22**:1413–1446.
5. Friedman A, Liu Y. Propagation of cracks in elastic media. *Archive for Rational Mechanics and Analysis* 1996; **136**(3):235–290.
6. Gurtin ME. On the energy release rate in quasi-static elastic crack propagation. *Journal of Elasticity* 1979; **9**(2):187–195.
7. Morozov NF. *Mathematical Foundation of Crack Theory*. Nauka: Moscow, 1984 (in Russian).
8. Rice JR. Elastic fracture mechanics concepts for interfacial crack. *Transactions on ASME Journal of Applied Mechanics* 1988; **55**:98–103.
9. Mazja WG, Nazarow SA, Plamenewski BA. *Asymptotische Theorie elliptischer Randwertaufgaben in singulär gestörten Gebieten*. Akademie-Verlag: Berlin, 1991.
10. Khludnev AM, Kovtunenko VA. *Analysis of Cracks in Solids*. WIT-Press: Southampton, Boston, 2000.
11. Sokolowski J, Zolesio J-P. *Introduction to Shape Optimization Shape Sensitivity Analysis*. Springer: Berlin, 1992.
12. Khludnev AM, Sokolowski J. The Griffith formula and the Cherepanov–Rice integral for crack problems with unilateral conditions in nonsmooth domains. *European Journal of Applied Mathematics* 1999; **10**:379–394.
13. Bach M, Khludnev AM, Kovtunenko VA. Derivatives of the energy functional for 2D-problems with a crack under Signorini and friction conditions. *Mathematical Methods in Applied Sciences* 2000; **23**:515–534.
14. Kovtunenko VA. Sensitivity of cracks in 2D-Lamé problem via material derivatives. *Journal of Applied Mathematics and Physics* (*ZAMP*) 2001; **52**(6):1071–1087.
15. Kovtunenko VA. Sensitivity of interfacial cracks to non-linear crack front perturbations. *Journal of Applied Mathematics and Mechanics* (*ZAMM*) 2002; **82**(6):387–398.
16. Bach M, Kovtunenko VA, Sukhorukov IV. Numerical validation of the shape optimization approach to quasi-static crack propagation. *SFB404 Bericht*, 2000/29, Universität Stuttgart, 2000.

